UNIVERSITY OF LEEDS

This is a repository copy of *Mechanism selection for spontaneous grain refinement in undercooled metallic melts*.

White Rose Research Online URL for this paper:
http://eprints.whiterose.ac.uk/79856/

Version: Accepted Version

Article:
Castle, EG, Mullis, AM and Cochrane, RF (2014) Mechanism selection for spontaneous grain refinement in undercooled metallic melts. Acta Materialia, 77. 76 - 84. ISSN 1359-6454

https://doi.org/10.1016/j.actamat.2014.05.043

Reuse
Unless indicated otherwise, fulltext items are protected by copyright with all rights reserved. The copyright exception in section 29 of the Copyright, Designs and Patents Act 1988 allows the making of a single copy solely for the purpose of non-commercial research or private study within the limits of fair dealing. The publisher or other rights-holder may allow further reproduction and re-use of this version - refer to the White Rose Research Online record for this item. Where records identify the publisher as the copyright holder, users can verify any specific terms of use on the publisher's website.

Takedown
If you consider content in White Rose Research Online to be in breach of UK law, please notify us by emailing eprints@whiterose.ac.uk including the URL of the record and the reason for the withdrawal request.

White Rose university consortium
Universities of Leeds, Sheffield & York

eprints@whiterose.ac.uk
https://eprints.whiterose.ac.uk/

Mechanism selection for spontaneous grain refinement in undercooled metallic melts

Elinor G. Castle[a], Andrew M. Mullis[b], Robert F. Cochrane[c]

[a]Institute of Materials Research, University of Leeds, Leeds LS2 9JT, UK.
pm07egc@leeds.ac.uk

[b]Institute of Materials Research, University of Leeds, Leeds LS2 9JT, UK.
A.M.Mullis@leeds.ac.uk

[c]Institute of Materials Research, University of Leeds, Leeds LS2 9JT, UK.
R.F.Cochrane@leeds.ac.uk

Corresponding author:

Elinor Castle. IMR, School of Process, Environmental and Materials Engineering, Engineering building, University of Leeds, Leeds, LS2 9JT, UK.
pm07egc@leeds.ac.uk. +44(0)113 343 2391 or +44(0)7891519694.[1]

[1] Permanent address: Flat 9 Burton Lodge, 202 Worple Road, Wimbledon, SW20 8PN

Abstract

In a previous paper (Castle EG, Mullis AM, Cochrane RF, Acta Materialia 2014;66:378-387), we employed a melt fluxing technique to study the velocity-undercooling relationship and microstructural development of a Cu-8.9 wt.% Ni alloy in order to investigate the fundamental mechanism behind the rapid solidification phenomenon of 'spontaneous grain refinement'. A number of growth transitions were identified with increasing undercooling, including an extended dendrite orientation transition through: fully <100>-oriented → multiply-twinned, mixed <100>/<111>-oriented → fully <111>-oriented. Here, we present the results of an identical study into in to a Cu-Ni alloy of lower Ni content and observe a similar set of growth transitions, with some notable differences. In particular, a total of three distinct grain refinement mechanisms have been observed between the two alloys, including; recrystallisation, dendrite fragmentation and dendritic seaweed fragmentation. It appears that the mechanism selected depends strongly upon the original growth structure present, which we suggest is dictated by the balance between the capillary and kinetic anisotropies; with the addition of Ni to Cu either increasing the strength of the kinetic anisotropy, decreasing the strength of the capillary anisotropy, or a combination of both. The unambiguous identification of three different spontaneous grain refinement mechanisms in two closely related alloys is significant as it may help to resolve some of the debate surrounding the 'true' grain refinement mechanism.

Keywords: Rapid solidification; undercooling; dendrite growth; dendrite orientation transition; spontaneous grain refinement

1. Introduction

‘Spontaneous grain refinement’ is a rapid solidification phenomenon observed in metals, in which abrupt transitions between course columnar and fine equiaxed grain structures are observed at well-defined values of undercooling, ΔT^*. In general, for pure metals (e.g. [1-3]), one grain refinement transition is observed at high ΔT; whilst for alloys (e.g. [4-7]), two grain refinement transitions occur, with an additional transition at low ΔT and columnar growth stabilised at intermediate ΔT. First reported in 1959 by Walker [8] for bulk undercooled Ni, spontaneous grain refinement has received a large amount of interest, since it demonstrates that grain refinement can be achieved in a way which is intrinsic to the solidification process itself. This therefore provides an attractive alternative to the conventional chemical or mechanical means of producing grain refined metals, offering significant commercial potential. Furthermore, since the onset of spontaneous grain refinement alters or removes the original growth structure, continuous measurements of the original dendrite length scale cannot be made as a function of undercooling (and, by extension, growth velocity). This therefore presents problems for the modelling of rapid dendrite growth, since there is a subsequent lack of data on which to base and test mathematical models. As such, many studies have been undertaken in order to elucidate the fundamental mechanism behind spontaneous grain refinement. Theories have ranged from: cavitation in the melt, leading to copious nucleation ahead of the solid-liquid interface [8]; partial remelting of secondary and tertiary dendrite branches [9]; recrystallisation [2, 10, 11]; dendrite fragmentation [12-14]; surface energy driven remelting and fragmentation of dendrites [15] and; a transition to dendritic seaweed growth followed by rapid remelting at the split dendrite junctions during recalescence [16]. However, the contrasting and conflicting evidence

produced by different studies has resulted in a large amount of debate on the matter, with no individual model able to provide a complete explanation for the behaviour observed.

In a previous paper [17], we employed a containerless melt-fluxing technique to undercool and rapidly solidify a Cu-8.9 wt.% Ni alloy. A careful study of the evolution of microstructure and texture with increasing undercooling/solidification velocity was then undertaken in order to further elucidate the grain refinement mechanism. An extended transition in growth orientation was observed; with normal, <100>-oriented growth dominating at low ΔT and anomalous, <111>-oriented growth dominating at high ΔT. Within the intermediate undercooling range, the competing anisotropies of the two growth directions were observed to give rise to mixed-orientation dendrites, dendritic seaweed 'branches' and twinning; with several samples exhibiting multiply twinned growth [17]. Further analysis of these twinning relationships will be presented in a separate paper in due course. Upon the observed transition to fully <111>-oriented growth, a transition to a coarse dendritic grain structure was observed. This was coincident with a positive break in the gradient of the growth velocity vs. undercooling curve; indicating that the <111>-oriented growth was faster than the <100> growth it replaced. Microstructural analysis indicated that grain refinement at low undercooling had occurred via a recrystallisation mechanism, whilst at high undercooling, a partially grain refined sample was obtained, in which the substructure of the non-grain refined portion consisted of dendritic seaweed; suggesting that seaweed is the precursor to grain refinement at high undercooling in this alloy.

Such an extended transition in growth orientation had not previously been reported as a function of undercooling. Abrupt, growth velocity/undercooling-mediated switches in preferred growth orientation have been reported in transparent metal analogue systems [18, 19], in strongly faceting Ge-Fe [1] and in Cu-Sn [20]; and an extended 'Dendrite Orientation Transition' (DOT) has been experimentally and computationally observed by Dantzig et al. [21] as a function of increasing Zn content in Al. Here, <100>-oriented growth is observed for low Zn content and <110>-oriented growth is observed for high Zn content. At intermediate Zn concentrations, the close competition between the differently-directed anisotropies is observed to give rise to textured, seaweed-like structures. It is subsequently suggested that the weak anisotropy of the solid-liquid interfacial energy of Al is altered by the addition of Zn, which has a relatively high interfacial energy anisotropy. This reinforced the findings of Haxhimali et al. [22], who had previously reported that changes in the composition-dependant interfacial anisotropy parameters could lead to changes in preferred growth orientation; accounting for the atypical dendrite growth directions observed in some FCC alloys [23-26]. Within this work, an orientation selection map was produced; exhibiting a region of <100>-oriented growth, a region of <110>-oriented growth and a region of parameter space in between the two orientations in which 'hyperbranched' structures were observed. When the corresponding data of several pure FCC metals (from - [27]) were plotted onto this orientation selection map, it was shown that several of these metals lie close to the <100>-hyperbranched boundary – including Cu and Ni. This might therefore suggest that the growth orientation transition observed in our previously investigated Cu-Ni alloy may, at least in part, be due to the alteration of the interfacial energy anisotropy of Cu by the addition of Ni.

Alternatively, the orientation transition may be due to the increasing influence of the kinetic anisotropy over the solidification process as the growth velocity is increased. If sufficient influence is gained, the kinetic anisotropy may compete with, and then override, the capillary anisotropy; perhaps accounting for the observation of a mixed orientation regime, followed by the transition to fully <111> oriented growth. At the highest velocities recorded; the subsequent, strongly dominant kinetic anisotropy may then account for the final observed transition to seaweed growth. Bragard et al. [28] have shown that a sufficiently high kinetic anisotropy can lead to a transition to dendritic seaweed growth in the vicinity of the ΔT^* transition; however, it is noted that this is only when set to unrealistically high values. As such, our observation of seaweed growth suggests that either the model is in some way flawed, or that other factors may be contributing to the development of these growth instabilities. Since it has been shown that the effective crystal anisotropy of the <111> orientation is weak [29] it may be that the transition to this orientation, in combination with the increased kinetic influence, is enough to induce a transition to seaweed growth. Alternatively, it may be that a combination of increased kinetic effect and an altered interfacial energy anisotropy (as discussed above with regards to the work of Haxhimali [22] and Dantzig et al. [21]) is giving rise to the growth orientation transition and seaweed growth observed in our previous work.

In order to investigate our previous findings further, the present report details the results of an identical study into a Cu-Ni alloy of lower Ni content. A comparison of the results of the two studies is then given, in order to examine the effect of Ni concentration on the observed growth transitions, and a discussion is subsequently provided in consideration of the possible contributing factors to the behaviour observed.

2. Material and methods

The methodology employed in the present report to prepare, characterise, undercool and analyse samples of Cu-Ni alloy is near identical to that of our previous study. Hence, whilst a general outline is presented herein, the reader is referred to the former paper [17] for a more detailed description of the experimental method.

High purity Cu and Ni powders (99.999 % metals basis from Alfa Aesar) were weighed and mixed to a composition of Cu-5 at% Ni (Cu-4.63 wt.% Ni), compacted into pellets and then melted to produce a slug of alloy. X-ray diffraction (XRD) patterns obtained from the alloy confirmed that a sufficient degree of homogeneity had been achieved via this method, and indicated the presence of a small amount of NiO. Inductively coupled plasma – optical emission spectroscopy (ICP-OES) analysis[2] confirmed a final composition of Cu-3.98 wt.% Ni, whilst light element combustion (LECO®) analysis indicated a residual oxygen concentration of 0.241 wt.%. A 1.826 % weight loss was noted following arc melting, which can account for the discrepancy in the final alloy composition. As discussed in our previous paper, the small amount of oxygen/NiO identified in the sample is not considered to be a concern, since it is expected to partition out ahead of the solid liquid interface and into the glass flux during successive fluxing cycles. For example, Mulls et al. [30] reported a decrease in the residual oxygen content of as-received high purity Cu by one order of magnitude following melt fluxing.

[2] ICP-OES and LECO® analysis performed by LSM Analytical Services

Small, 5-7 mm diameter droplets of the prepared alloy slug were then ultrasonically cleaned in a warm aqueous solution of ammonium peroxodisulphate to remove any surface oxides or impurities. Each sample was then placed in a small fused-silica crucible and subjected to repeated heating and cooling cycles via the induction heating of a graphite susceptor. Temperature was closely monitored via an r-type thermocouple positioned at the base of the crucible. Each experiment was performed under a 500 mbar inert N_2 atmosphere, contained within a stainless steel vacuum chamber. Samples were isolated from the crucible walls by suspension in a dewatered 40% Na_2SiO_3 – 60% B_2O_3 glass flux, in order to significantly reduce the number of potent heterogeneous nucleants present and subsequently attain a large degree of undercooling. Each cycle consisted of superheating to 130 K above the equilibrium liquidus temperature of the alloy (T_l = 1385 K), holding at this temperature for 15 min and then slow cooling, at a rate of 10 K min^{-1}, until the sample spontaneously nucleated. The temperature at which recalescence was observed was then recorded in order to calculate the degree of undercooling. *In situ* observations of the solidification process are made possible through careful arrangement of the equipment; with a viewing window incorporated into the vacuum chamber and slots cut into the susceptor and alumina radiation shield at the height of the sample. During solidification from the undercooled melt, the progression of the solidification front could therefore be tracked during recalescence using a high speed camera (up to 15 000 fps); and a solidification velocity, V, calculated from the resulting images. As such, each heating/cooling cycle generates a V- ΔT data point, allowing the V- ΔT relationship to be examined. Each experiment consisted of approximately 6 cycles and generated one undercooled droplet for further analysis.

Samples, undercooled to varied amounts, were then subjected to microstructural and texture analysis using: light microscopy, SEM secondary-electron imaging and XRD pole figure analysis, as described in our previous paper. The evolution of microstructure with increasing undercooling could then be assessed and compared to the high-Ni alloy previously investigated.

3. Results

3.1. Melt fluxing investigation into the Cu-3.98 wt.% Ni alloy

The velocity-undercooling curve obtained for the Cu-3.98 wt.% Ni alloy is shown in figure 1. Error bars have been plotted, taking into account the human and instrumental error associated with the calculation of the solidification velocity from high-speed images of the growth front. These are represented as ± 20 % of the reported value for consistency with our previous work. Maximum undercoolings of up to $\Delta T = 216$ K have been achieved, corresponding to growth velocities of up to 93 m s^{-1}. A power law trend has been fitted to the full data set for ease of comparison with the high-Ni alloy previously reported. A positive departure of the data from this trend can be seen at undercoolings of around $\Delta T \approx 200$ K ($V \approx 40$ m s^{-1}), consistent with that reported for the high-Ni alloy. However, for this data set, it is difficult to unambiguously define the position of the break in the trend, based upon the linear plot of the data. For both this alloy and the Cu-8.9 wt.% Ni alloy, the power law trend initially proceeds with a ΔT exponent of close to 2; hence a V - ΔT^2 plot has been investigated for the data sets of both the high and low Ni alloys (figure 2). This plot reveals a good degree of proportionality between V and ΔT^2, and indicates clear positive breaks in both data sets.

For the Cu-3.98 wt.% Ni alloy, the break occurs at approximately $\Delta T \approx 192$ K ($V \approx 31$ m s^{-1}); whilst, for the Cu-8.9 wt.% Ni alloy, the break occurs at around $\Delta T \approx 204$ K ($V \approx 29$ m s^{-1}). The overall V - ΔT^2 trend for both alloys is very similar, and appears to be shifted to lower undercoolings with a decrease in Ni content. Since the break in the V - ΔT trend of the high-Ni alloy was found to correspond to a transition to <111>-oriented growth, the existence of a similar break in the presently investigated low-Ni alloy, suggests that a similar transition may have taken place. A positive break due to the transition to <111> growth is further supported by the work of Gudgel and Jackson [19], who noted that a similar transition, occurring in an FCC metal analogue system, was accompanied by a sharpening of the dendrite tip and subsequent increase in growth velocity.

In order to further investigate the presence of any growth transitions, a detailed examination of the microstructural and texture evolution with undercooling has been undertaken, the results of which are summarised in figure 1.

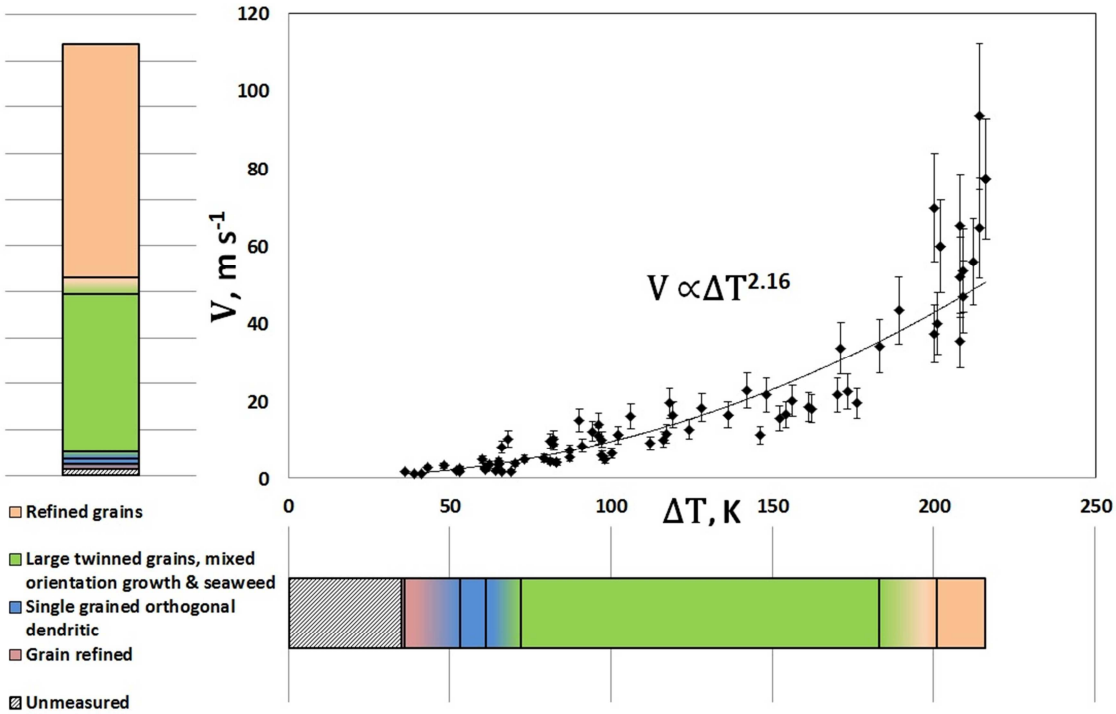

Figure 1. Growth velocity (V) as a function of undercooling (ΔT) and a summary of the growth transitions observed with increasing undercooling in Cu-3.98 wt.% Ni plotted against both ΔT and V. The uncertainty in the exact position of each transition is indicated by the regions in which there are colour gradients, which represent the extent of the unmeasured range of undercooling, i.e. no undercooled droplets have been examined within this range.

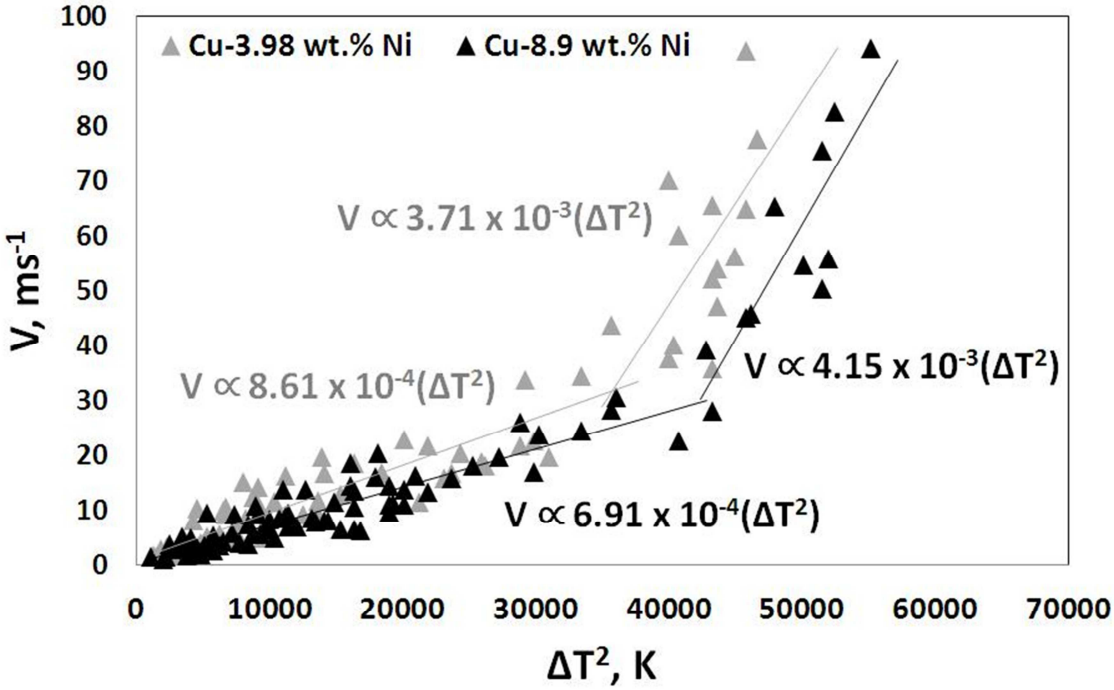

Figure 2. V - ΔT^2 plot for both Cu-3.98 wt.% Ni and Cu-8.9 wt.% Ni alloys.

3.1.1. Grain refined structures for $\Delta T \leq 36$ K

At very low undercooling, solidifying samples do not display any visible recalescence and hence measurements of undercooling and solidification velocity cannot be made. At the lowest undercooling detected ($\Delta T = 36$ K), a sample was obtained in which a grain refined microstructure is observed. It can be assumed that a region of stable dendrite growth precedes this grain refinement regime, based on the fact that stable dendrite growth would at least be expected under equilibrium growth conditions. Figure 3 shows the internal microstructure of this droplet, both at the surface and within the centre of it. Dendrite fragments can be seen at the surface, which appear to exhibit secondary arms at 90° to the primary; suggesting that normal, <100>-oriented growth took place initially. Within the centre of the droplet, a large grain structure consisting of small subgrains is observed – akin to that reported in the high-Ni alloy previously

investigated. However, in this instance, no continuous underlying dendritic substructure is observed. Instead, fragmented dendrite 'cores' are evident, with the low-angle subgrain boundaries most likely formed due to the slight misorientations between them. The {200} pole figure taken from this sample (figure 3 inset) indicates the presence of at least three unrelated grains, confirming the discontinuity of the substructure between them. As such, in contrast to the recrystallisation mechanism reported for the Cu-8.9 wt.% Ni alloy, the low undercooling region of grain refinement in this alloy appears to take place via the fragmentation of <100>-oriented dendrites.

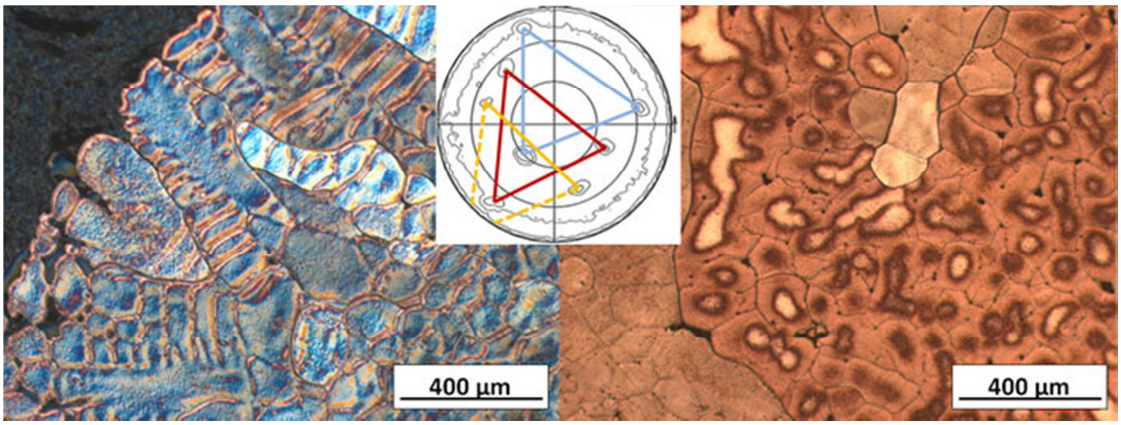

Figure 3. Micrographs of a randomly-sectioned Cu-3.98 wt.% Ni droplet undercooled by ΔT = 36 K. (Left) DIC image of fragmented dendrites at droplet surface; (right) bright field image of fragmented dendrite cores, large grains and fine subgrain boundaries at centre of droplet; (middle inset) {200} pole figure showing the presence of at least three unrelated grains.

3.1.1. Single grained <100>-oriented dendritic structures between 37 K ≤ ΔT < 72 K

The microstructure of undercooled droplets collected at ΔT = 53 K (figure 4) and ΔT = 61 K reveal a return to stable dendritic growth as undercooling is increased. The orthogonality of the secondary dendrite arms to the primary trunks suggests that growth

took place along a preferred <100> growth direction. Texture analysis confirms the single grain nature of these droplets, with only one set of poles observed on the {200} pole figure (figure 4 inset). This is in contrast to the high-Ni alloy previously investigated, which exhibited a transition to the '8-fold' mixed-orientation growth regime immediately following the first region of grain refinement.

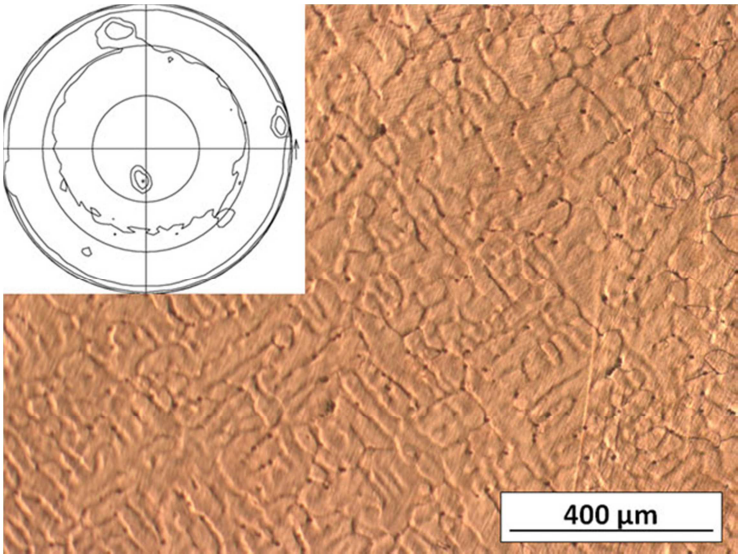

Figure 4. Optical bright field micrograph of a random section of the interior microstructure of a Cu-3.98 wt.% Ni droplet undercooled by $\Delta T = 53$ K; showing a single grain microstructure consisting of orthogonal, <100> type dendrites. The {200} pole figure taken from this sample is inset, showing one set of poles associated with the single grain morphology.

3.1.2. Mixed orientation structures between 72 K ≤ ΔT ≤ 200 K

As the undercooling is increased further a transition to a mixed orientation regime, similar to that reported for the high-Ni alloy, is observed; occurring somewhere between 61 K < $\Delta T \leq 72$ K. Up to (at least) $\Delta T \geq 183$ K, nucleation points could be observed on the surface of the droplets (figures 5 and 6). Dendrites emanating from these nucleation points exhibit features of mixed-orientation growth; with secondary arms growing at

both orthogonal and non-orthogonal angles to the primary branch. The seaweed branches reported in our previous paper are also observed within the mixed orientation regime of this alloy (figure 5 bottom, feature 2). However, a much broader range of split-branch morphologies are present; each of which initially stems from a diverging split primary dendrite branch and then develops inner secondary arms of varied morphologies, including: orthogonal and non-orthogonal dendritic (figure 5 top, features 1 & 2), parallel dendritic (figure 5 bottom, feature 1), and seaweed. In contrast to the high-Ni alloy, no distinct symmetry pattern can be explicitly deduced for any of the nucleation points observed, and therefore no ‘8-fold’ to ‘6-fold’ transition is seen. In our previous paper we suggested that this was indicative of the transition between <100>-dominant and <111>-dominant growth. However, with increasing undercooling, such a transition does still appear to be occurring; since pole figures obtained from samples at lower undercoolings exhibit strong poles near to the centre of the {200} plot (figure 7), whilst those at higher undercooling exhibit poles in the centre of the {111} plot (figure 6).

In addition, no instances of multiple twinning have been identified in any of the samples investigated for this alloy. Each sample, undercooled within the mixed-orientation regime and subjected to texture analysis was, however, found to be twinned about one of the {111} planes; an example of which can be seen from the inset pole figure of figure 6, a sample undercooled by $\Delta T = 148$ K prior to nucleation. Two sets of poles are evident from this pole figure, indicating the presence of at least two large grains, with one pole shared between the two. Since this sample was sectioned parallel to the growth direction and the shared pole is not the one observed at the centre of the pole figure, this suggests that the sample is twinned about one of the secondary dendrite growth

directions. As growth has proceeded from a single point, this suggests that twinning has occurred during the growth of a secondary dendrite arm. The interior microstructure of this droplet is also shown in figure 6, and is representative of the large dendritic/seaweed grain structure observed in samples undercooled within the mixed-orientation regime. Wavy grain boundaries are observed, with the substructure appearing to traverse these, and the occasional ‘floating’ grain (as indicated by the arrow) is seen, indicative of significant grain boundary migration in the solid state. Since grain boundary migration is enhanced at elevated temperatures, it is likely that this occurred during cooling from the high temperatures reached during recalescence.

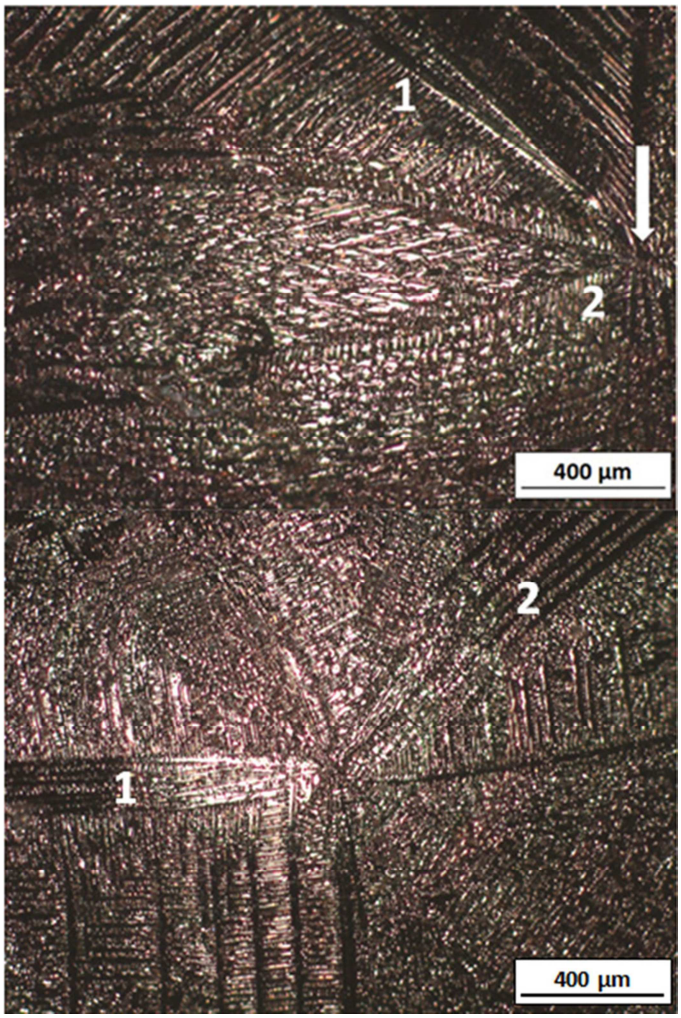

Figure 5. (Top) Nucleation point (arrow) on the surface of a Cu-3.98 wt.% Ni droplet undercooled by ΔT = 119 K, demonstrating two distinct forms of diverging split primary dendrite branch (features 1 and 2). (Bottom) Nucleation point on the surface of a droplet undercooled by ΔT = 117 K showing a split primary dendrite branch in which inner secondary arms bend to grow parallel to the primary (feature 1) and a <100>-type seaweed branch, as identified in our previous paper (feature 2).

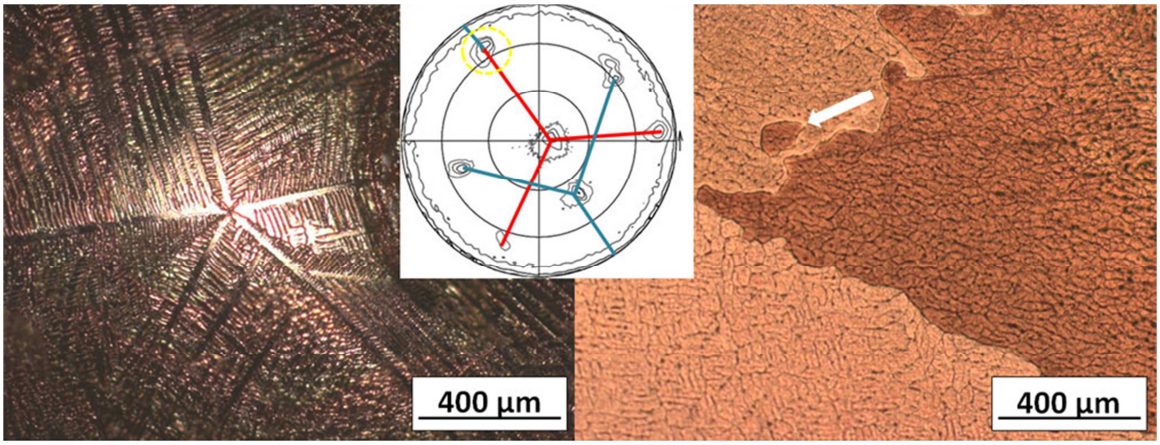

Figure 6. (Left) Through-focused micrograph of the nucleation point evident on the surface of a Cu-3.98 wt.% Ni droplet undercooled by ΔT = 148 K. (Right) Optical micrograph of the interior microstructure of the droplet, showing coarse dendritic/seaweed grains and significant grain boundary migration, as indicated by the wavy grain boundaries and the presence of a 'floating' grain (white arrow). (Inset middle) Associated {111} pole figure indicating the presence of at least two grains, which are twinned about one of the {111} planes (indicated by the yellow circle), and where a strong pole is observed in the centre; indicating a dominant <111> growth orientation.

Figure 7. {200} pole figure obtained from a Cu-3.98 wt.% Ni droplet undercooled by ΔT = 100 K and sectioned (as close as possible to) parallel to the growth direction, showing a sharp pole close to the centre, indicating a dominant <100> growth direction.

3.1.3. Grain refined structures for ΔT > 184 K

As the undercooling is increased, a spontaneous grain refinement transition occurs somewhere within the undercooling range 184 K ≤ ΔT ≤ 201 K, coincident with the break in the V - ΔT curve. Since a dominant <111> orientation was observed in the mixed orientation regime prior to this transition, and since there is a positive break in the V - ΔT relationship, this suggests that a transition to faster, fully <111>-oriented growth has taken place. However, as the original growth structure has been replaced by the refined grains, this is difficult to confirm microstructurally. Droplets collected between ΔT = 201 K and the maximum achieved undercooling of ΔT = 216 K are all grain refined and exhibit similar microstructures. The interior and exterior microstructure of the ΔT = 216 K droplet is shown in figure 8, along with the {111} pole figure obtained from this sample. This pole figure shows numerous random, unrelated sets of poles, confirming the presence of a large number of randomly oriented grains. The interior microstructure of this droplet (figure 8, right) reveals an average equiaxed grain size of around 200 μm in diameter. The substructure of these grains appears to traverse some of the grain boundaries, but not all, and is dendritic in nature. However, the morphology of these dendrites is unclear, making it difficult to determine the character of the original growth structure. From the micrograph of the droplets' surface topography (figure 8, left) a fragmented dendrite structure can be seen; with each fragment constituting a single grain. It therefore appears that the high undercooling region of grain refinement in this alloy arises from the fragmentation of dendrites; which, as discussed, are most likely of <111> orientation. This is in contrast to the high-Ni alloy previously investigated; in which a large, unrefined grain structure was

observed upon the transition to fully <111>-oriented growth, and whereby the precursor to spontaneous grain refinement was found to be dendritic seaweed.

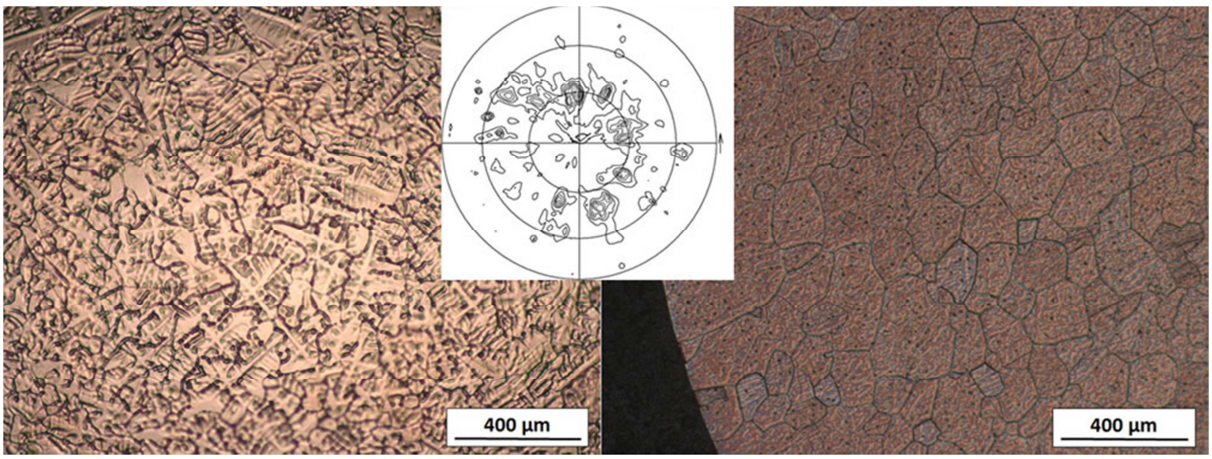

Figure 8. (Left) Light microscope image of the fragmented dendrite structure observed on the surface of a grain refined Cu-3.98 wt.% Ni droplet undercooled by ΔT = 216 K. (Right) DIC micrograph of the interior grain structure of the droplet, showing refined dendritic grains. (Inset middle) {111} pole figure obtained from the sample showing a large number of poles.

4. Discussion

In summary, the growth transitions observed in the present study of a Cu-3.98 wt.% Ni alloy are similar to that observed in the Cu-8.9 wt.% Ni alloy previously investigated [17]; with an extended transition in growth orientation, from <100>-oriented at low undercooling to <111>-oriented at high undercooling. However, there are a few key differences worth noting. With increasing undercooling, the low-Ni alloy appears to transition through:

- Single-grained <100> dendritic → grain refined from a fragmented <100> dendrite precursor → single-grained <100> dendritic → large, mixed

<100>/<111> oriented, twinned grains →grain refined from a fragmented <111> dendrite precursor;

whilst the high-Ni alloy transitions through:

- Single-grained <100> dendritic → grain refined following recrystallisation → large, mixed <100>/<111> oriented, twinned/multiply-twinned grains → coarse dendritic grains from <111> precursor → grain refinement from dendritic seaweed precursor.

Thus, three distinct grain refinement mechanisms have been identified in the two closely related alloys. Firstly, spontaneous grain refinement in the low-Ni alloy appears to be consistent with the model of Schwarz et al. [15], since two grain refinement transitions are observed to arise from the fragmentation of dendrites. The Schwarz model is based upon the LKT theory of dendrite growth [31]; in which the dendrite tip radius passes through a local minimum followed by a local maximum with increasing undercooling, as the transfer between solutally and thermally-controlled growth occurs. Schwarz et al. subsequently incorporate the stability analysis of Karma [32] to propose that grain refinement occurs when the dendrite tip radius falls below a certain value, allowing the side branches to fragment during recalescence. This theory therefore provides a feasible explanation for the two grain refinement transitions observed in alloys, as opposed to the single transition observed in pure metals. As such, it remains the most widely accepted theory for spontaneous grain refinement, despite having come under some scrutiny for its reliance on a model of dendritic growth that does not incorporate anisotropy and dynamics of the remelting instability [33]. In the case of the low-Ni alloy, grain refinement appears to occur from the fragmentation of refined

<100> dendrites at low undercooling, and, following the orientation transition, from the fragmentation of refined <111> dendrites at high undercooling.

A second grain refinement mechanism of recrystallisation has then been observed at low undercooling in the high-Ni alloy, consistent with a number of other reports [2, 10, 11]. The difference between the fragmentation mechanism observed in the low-Ni alloy and the recrystallisation mechanism observed in the high-Ni alloy appears to arise from the difference in the original growth structure. In the low-Ni alloy, stable <100>-oriented growth is observed well beyond the first grain refinement transition, suggesting that the precursor in this case is <100> dendrites; in which case the greatest driving force for grain refinement seems to be the fragmentation of these dendrites following a gradual scale refinement. However, in the high-Ni alloy, there is an abrupt transition from the grain refined to the mixed-orientation regime, suggesting that the two regimes may coincide. Thus, the precursor to grain refinement in this instance would be mixed-orientation dendrites; the presence of which most likely indicates the existence of a high dislocation density, thereby providing sufficient driving force for a recovery/recrystallisation process in place of refinement and fragmentation.

Finally, the remelting and fragmentation of a seaweed precursor appears to be the most likely mechanism for spontaneous grain refinement at high undercooling in the high-Ni alloy; in line with that proposed by Mullis et al. [16]. In order to understand why seaweed is observed for the high Ni alloy only, a consideration of the effect of Ni content is required. Since the addition of more Ni to Cu shifts the mixed orientation regime to lower undercoolings (with respect to the first grain refinement transition), and

since this brings about a transition to seaweed growth, it is suggested that the addition of Ni either:

1. Decreases the strength of the capillary anisotropy;
2. Increases the strength of the kinetic anisotropy, or;
3. A combination of both 1 & 2.

This would result in a closer competition between the two anisotropies; shifting the range over which they compete (the mixed-orientation regime) to lower undercoolings with the addition of more Ni.

In the first instance, a decrease in the strength of the capillary anisotropy would suggest that the interfacial energy anisotropy of Cu is being altered by the addition of Ni – an idea supported by the work of Haxhimali et al. [22] and Dantzig et al. [21], outlined in the introduction.

In the second case, an increased kinetic anisotropy might occur due to the need to incorporate more Ni into the growing crystal solid. Since a high growth velocity clearly favours <111>-oriented growth, this must therefore be a favoured kinetic direction. One explanation for this could be that the atomic radius of Ni is slightly smaller than that of Cu (124.6 pm and 127.8 pm respectively). This is perhaps close enough to retain the FCC crystal structure but sufficiently different to roughen the close-packed {111} planes; thereby enhancing atomic attachment kinetics along them. As discussed in the introduction, the work of Bragard et al. [28] has shown that a sufficiently high kinetic anisotropy can lead to a transition to dendritic seaweed growth. Hence, the observation of a seaweed precursor to the ΔT^* transition in the high-Ni alloy (and not in the low-Ni alloy) supports the notion of an enhanced kinetic anisotropy due to the addition of Ni.

The addition of more Ni to Cu therefore appears to shift the seaweed transition to lower, more achievable values of undercooling; which may subsequently alter the precursor to spontaneous grain refinement. The notion of an increased kinetic effect might also explain why multiple twinning is only observed for the high-Ni alloy, since this may result in an increased probability of developing stacking faults during growth.

It is, of course, possible that both interfacial energy and kinetic effects are playing some part in the complex behaviour observed between the two alloys. The unambiguous identification of several different grain refinement mechanisms in two closely related alloys is significant, since it may help to resolve some of the debate surrounding the 'true' spontaneous grain refinement mechanism. In reality it appears that there are a number of potential mechanisms, the selection of which appears dependent upon the original growth structure present; which in turn is dictated by a number of contributing factors to the complex problem of rapid dendrite growth.

5. Conclusions

Following the identification of a number of complex growth transitions with increased undercooling in a Cu-8.9 wt.% Ni alloy [17], an identical study had been undertaken into an alloy of lower Ni content (Cu-3.98 wt.% Ni) in order to investigate the effect of solute upon the observed growth transitions. Once again, an extended transition between <100>-oriented dendrite growth at low undercooling and <111>-oriented growth at high undercooling has been observed, with a mixed-orientation regime existing at intermediate undercooling. In contrast to the high-Ni alloy, however, stable <100> growth is observed up to undercoolings well beyond the first grain refinement transition, with a shift of the mixed orientation regime to higher undercoolings. As a

result, the precursor to grain refinement at low undercooling appears to be stable <100>-oriented dendrites, resulting in a fragmentation mechanism. This is in contrast to the recrystallisation mechanism observed in the high-Ni alloy; which arises from the existence of a mixed-orientation dendrite precursor, due to a coincidence of the mixed orientation regime with the grain refinement regime. At high undercooling, grain refinement in the low-Ni alloy is also observed to occur following the fragmentation of <111>-oriented dendrites. This is again in contrast to the high-Ni alloy, in which dendritic seaweed was identified as the most likely precursor to spontaneous grain refinement. It is postulated that the observed shift in the mixed orientation regime and seaweed transition to lower undercoolings with increased Ni content is due to either: an increase in the strength of the kinetic anisotropy; a decrease in the strength of the capillary anisotropy, or; a combination of both. This would lead to a closer competition between the two anisotropies; accounting for the observed growth transitions, their influence over the microstructure and the subsequent impact of this upon the grain refinement mechanism. The identification of, and explanation for, three distinct grain refinement mechanisms in two closely related alloys may help to clear some of the debate surrounding the ‘true’ mechanism of spontaneous grain refinement.

References

[1] Battersby SE, Cochrane RF, Mullis AM. Journal of Materials Science 1999;34:2049.

[2] Dragnevski KI, Cochrane RF, Mullis AM. Materials Science and Engineering A 2004;375-377:479.

[3] Li D, Eckler K, Herlach DM. Journal of Crystal Growth 1996;160:59.

[4] Li D, Eckler K, Herlach DM. Acta Materialia 1996;44:2437.

[5] Li S, Wang H-f, Liu F. Transactions of Nonferrous Metals Society of China 2013;23:3265.

[6] Li JF, Jie WQ, Yang GC, Zhou YH. Acta Materialia 2002;50:1797.

[7] Cochrane RF, Battersby SE, Mullis AM. Materials Science and Engineering: A 2001;304-306:262.

[8] Walker JL, editor The physical chemistry of process metallurgy, part 2. New York: Interscience, 1959.

[9] Jackson KA, Hunt JD, Uhlmann DR, Seward TP. Trans. TMS-AIME 1966;236:149.

[10] Southin RT, Weston GM. Journal of the Australian Institute of Metals 1973;18:74.

[11] Ovsiyenko DE, Maslov VV, Alfintsev GA. Journal of Russian Metallurgy 1974:66.

[12] Kattamis TZ, Flemings MC. Mod. Casting 1967;52.

[13] Chen YZ, Liu F, Yang GC, Liu N, Yang CL, Xie H, Zhou YH. Materials Characterization 2008;59:412.

[14] Kobayashi KF, Shingu PH. Journal of Materials Science 1988;23:2157.

[15] Schwarz M, Karma A, Eckler K, Herlach DM. Physical Review Letters 1994;73:1380.

[16] Mullis AM, Dragnevski KI, Cochrane RF. Materials Science and Engineering A 2004;375-377:157.

[17] Castle EG, Mullis AM, Cochrane RF. Acta Materialia 2014;66:378.

[18] Sawada Y. Physica A: Statistical Mechanics and its Applications 1986;140:134.

[19] Gudgel KA, Jackson KA. Journal of Crystal Growth 2001;225:264.

[20] Dragnevski KI, Cochrane RF, Mullis AM. Metallurgical and Materials Transactions A 2004;35:3211.

[21] Dantzig JA, Napoli PD, Friedli J, Rappaz M. Metallurgical and Materials Transactions A 2013;44.

[22] Haxhimali T, Karma A, Gonzales F, Rappaz M. Nat Mater 2006;5:660.

[23] Henry S, Rappaz M, Jarry P, Jouneau PH. Metallurgical and Materials Transactions A 1997;28:207.

[24] Henry S, Rappaz M, Jarry P. Metallurgical and Materials Transactions A 1998;29:2807.

[25] Henry S, Minghetti T, Rappaz M. Acta Materialia 1998;46:6431.

[26] Sémoroz A, Durandet Y, Rappaz M. Acta Materialia 2001;49:529.

[27] Hoyt JJ, Asta M, Karma A. Materials Science and Engineering R: Reports 2003;41:121.

[28] Bragard J, Karma A, Lee Y, Plapp M. Interface Science 2002;10:121.

[29] Akamatsu S, Faivre G, Ihle T. Physical Review E 1995;51:4751.

[30] Mullis AM, Dragnevski KI, Cochrane RF. Materials Science and Engineering: A 2004;375–377:547.

[31] Lipton J, Kurz W, Trivedi R. Acta Metallurgica 1987;35:957.

[32] Karma A, Rappel W-J. Physical Review E 1998;57:4323.

[33] Mullis AM, Cochrane RF. International Journal of Non-Equilibrium Processing 2000;11:283.

List of Figure Captions:

Figure 1. Growth velocity (V) as a function of undercooling (ΔT) and a summary of the growth transitions observed with increasing undercooling in Cu-3.98 wt.% Ni plotted against both ΔT and V. The uncertainty in the exact position of each transition is indicated by the regions in which there are colour gradients, which represent the extent of the unmeasured range of undercooling, i.e. no undercooled droplets have been examined within this range.

Figure 2. V - ΔT^2 plot for both Cu-3.98 wt.% Ni and Cu-8.9 wt.% Ni alloys.

Figure 3. Micrographs of a randomly-sectioned Cu-3.98 wt.% Ni droplet undercooled by ΔT = 36 K. (Left) DIC image of fragmented dendrites at droplet surface; (right) bright field image of fragmented dendrite cores, large grains and fine subgrain boundaries at centre of droplet; (middle inset) {200} pole figure showing the presence of at least three unrelated grains.

Figure 4. Optical bright field micrograph of a random section of the interior microstructure of a Cu-3.98 wt.% Ni droplet undercooled by ΔT = 53 K; showing a single grain microstructure consisting of orthogonal, <100> type dendrites. The {200} pole figure taken from this sample is inset, showing one set of poles associated with the single grain morphology.

Figure 5. (Top) Nucleation point (arrow) on the surface of a Cu-3.98 wt.% Ni droplet undercooled by ΔT = 119 K, demonstrating two distinct forms of diverging split primary dendrite branch (features 1 and 2). (Bottom) Nucleation point on the surface of a droplet undercooled by ΔT = 117 K showing a split primary dendrite branch in which inner secondary arms bend to grow parallel to the primary (feature 1) and a <100>-type seaweed branch, as identified in our previous paper (feature 2).

Figure 6. (Left) Through-focused micrograph of the nucleation point evident on the surface of a Cu-3.98 wt.% Ni droplet undercooled by ΔT = 148 K. (Right) Optical micrograph of the interior microstructure of the droplet, showing coarse dendritic/seaweed grains and significant grain boundary migration, as indicated by the wavy grain boundaries and the presence of a 'floating' grain (white arrow). (Inset middle) Associated {111} pole figure indicating the presence of at least two grains, which are twinned about one of the {111} planes (indicated by the yellow circle), and where a strong pole is observed in the centre; indicating a dominant <111> growth orientation.

Figure 7. {200} pole figure obtained from a Cu-3.98 wt.% Ni droplet undercooled by ΔT = 100 K and sectioned (as close as possible to) parallel to the growth direction, showing a sharp pole close to the centre, indicating a dominant <100> growth direction.

Figure 8. (Left) Light microscope image of the fragmented dendrite structure observed on the surface of a grain refined Cu-3.98 wt.% Ni droplet undercooled by ΔT = 216 K. (Right) DIC micrograph of the interior grain structure of the droplet, showing refined dendritic grains. (Inset middle) {111} pole figure obtained from the sample showing a large number of poles.